

Showcasing research from Professor Jyotirmayee Dash's laboratory, School of Chemical Sciences, Indian Association for the Cultivation of Science (IACS), Kolkata, India.

In situ formation of transcriptional modulators using non-canonical DNA i-motifs

i-Motif DNA immobilized magnetic nanoparticles assemble the best binders via selection followed by *in situ* cycloaddition. The generated i-motif specific ligands modulate the transcription of cellular oncogenes.

We acknowledge Mr. Gopal Krishna Manna, IACS for his help with the preparation of the cover art.





Chemical Science



EDGE ARTICLE

View Article Online
View Journal | View Issue



Cite this: Chem. Sci., 2020, 11, 2058

All publication charges for this article have been paid for by the Royal Society of Chemistry

Received 4th September 2019 Accepted 28th January 2020

DOI: 10.1039/d0sc00514b

rsc.li/chemical-science

In situ formation of transcriptional modulators using non-canonical DNA i-motifs†‡

Puja Saha,^a Deepanjan Panda,^a Diana Müller,^b Arunabha Maity,^a Harald Schwalbe lob and Jyotirmayee Dash to *a

Non-canonical DNA i-motifs and G-quadruplexes are postulated as genetic switches for the transcriptional regulation of proto-oncogenes. However, in comparison to G-quadruplexes, the therapeutic potential of imotifs is less explored. The development of i-motif selective ligands by conventional approaches is challenging due to the structural complexity of i-motifs. The target guided synthetic (TGS) approach involving in situ cycloaddition could provide specific ligands for these dynamic DNA structures. Herein, we have used i-motif forming C-rich DNA and their complementary G-quadruplex forming DNA sequences of c-MYC and BCL2 promoter regions as well as a control self-complementary duplex DNA sequence as the templates to generate selective ligands from a pool of reactive azide-alkyne building blocks. In our approach, thiolated DNA targets are immobilized on the surface of gold-coated iron nanoparticles to enable efficient isolation of the newly generated ligands from the solution mixture by simple magnetic decantation. The combinatorial in situ cycloaddition generated cell-membrane permeable triazole leads for respective DNA targets (c-MYC and BCL2 i-motifs and G-quadruplexes) that selectively promote their formation. In vitro cellular studies reveal that the c-MYC i-motif and Gquadruplex leads downregulate c-MYC gene expression whereas the BCL2 i-motif lead upregulates and the BCL2 G-quadruplex lead represses BCL2 gene expression. The TGS strategy using i-motif DNA nanotemplates represents a promising platform for the direct in situ formation of i-motif specific ligands for therapeutic intervention.

Introduction

Non-canonical DNA i-motifs have recently emerged as molecular switches that control cellular transcription of several protooncogenes¹⁻³ like c-MYC, ^{4,5} BCL2, ^{6,7} $PDGFR\text{-}\beta$, ⁸ KRAS, ⁹ $HRAS^{10}$, $VEGF^{11}$, RET^{12} and Rb. ¹³ The tetraplex structure of an i-motif consists of two interspersed C-rich duplexes zipped together by intercalated hemiprotonated $C^+\cdot C$ base pairing at acidic pH. ¹⁴⁻¹⁶ The pH responsive structure and reversible conformational switching properties of i-motifs have been potentially used in DNA nanotechnology. ¹⁷⁻²⁰ However, i-motifs have been less investigated for designing ligands for therapeutics ²¹⁻²³ as compared to complementary G-quadruplexes (G_4 s) that have been well studied in the past decade. ²⁴⁻²⁶ The reported i-motif ligands such as the cationic porphyrin TmPyP4, ²⁷

phenanthroline derivatives,28 neomycin-perylene conjugates,29 crystal violet,30 Thioflavin T31,32 and berberine33 do not show significant selectivity for i-motif structures over duplex and quadruplex structures. In subsequent years, Hurley and coworkers identified a cholestane derivative as a potent and specific i-motif binder that can provide an approach for regulating BCL2 transcription in cancer cells.7 At present, only a couple of i-motif specific ligands e.g., the type II topoisomerase inhibitor mitoxantrone,34 peptidomimetic ligands,35 benzothiophene derivatives⁸ and acridone derivatives³⁶ have been tested in the cellular system. In a recent study, Dzatko et al. performed state of-the-art in-cell NMR spectroscopy to establish that i-motifs remain stable in the complex cellular environment of live mammalian cells.37 Moreover, the recent breakthrough discovery of the in vivo existence of i-motif structures in the nuclei of human cells by Christ and Dinger's group illustrates the therapeutic potential of i-motifs.³⁸ However, the development of selective ligands for i-motifs is difficult and challenging as i-motifs share a similar four stranded structural topology with quadruplexes. We herein demonstrate target guided in situ cycloaddition using i-motif linked gold coated magnetic nanoparticles as templates to generate selective ligands for i-motifs over G4s and double stranded DNA (dsDNA). The targetguided synthesis (TGS) using azide-alkyne cycloaddition (in

[&]quot;School of Chemical Sciences, Indian Association for the Cultivation of Science, Jadavpur, Kolkata-700032, India. E-mail: ocjd@iacs.res.in

^bInstitute of Organic Chemistry and Chemical Biology, Center for Biomolecular Magnetic Resonance (BMRZ), Goethe University, Max-von-Laue Strasse 7, Frankfurt, D-60438, Germany

 $[\]dagger$ This work is dedicated to Professor Hans-Ulrich Reissig on the occasion of his $70^{\rm th}$ birthday.

[‡] Electronic supplementary information (ESI) available. See DOI: 10.1039/d0sc00514b

Edge Article Chemical Science

situ click chemistry) is a powerful fragment-based drug design strategy in which the target directly templates the ligation of appropriate reactive fragments to generate high affinity targetspecific compounds. This method has been elegantly used for the discovery of potent binders for protein targets.³⁹⁻⁴² In comparison, only a few nucleic acid targets are used as templates like duplex DNA,43 DNA and RNA quadruplexes44,45 and $(CCUG)_n$ repeat RNAs⁴⁶ to generate selective ligands.

In this study, we have immobilized i-motifs present in *c-MYC* and BCL2 gene promoters on the surface of gold-coated magnetic nanoparticles (i-motif DNA nanotemplates) to enable efficient isolation and identification of selective triazole ligands from a library of azide and alkyne building blocks. In this approach, the DNA nanotemplates would capture the newly assembled triazole products that could be easily separated from the DNA templates by magnetic decantation. In addition, complementary c-MYC and BCL2 G-quadruplexes as well as double stranded DNA targets have been used as control DNA templates. The binding affinity, selectivity and gene regulatory activities of triazole leads for G-quadruplexes and i-motifs have been evaluated by using different biophysical and cell-based biological assays.

Results and discussion

Preparation and characterization of DNA nanotemplates

Thiolated i-motif forming C-rich sequences present in the promoter regions of c-MYC and BCL2 genes were grafted on the surface of gold-coated magnetic nanoparticles (Au@Fe₃O₄) using thiol-gold chemistry to obtain c-MYC C4 · Au@Fe3O4 and BCL2 C₄·Au@Fe₃O₄ nanotemplates (Fig. 1).

The attachment of i-motif DNAs on Au@Fe3O4 NPs was confirmed by the peak at 260 nm for DNA along with the characteristic SPR peak of Au at \sim 550 nm in the UV-Vis spectrum in 10 mM sodium cacodylate buffer, pH 5.5 (Fig. 2a and b). TEM imaging revealed that i-motif DNA linked NPs are

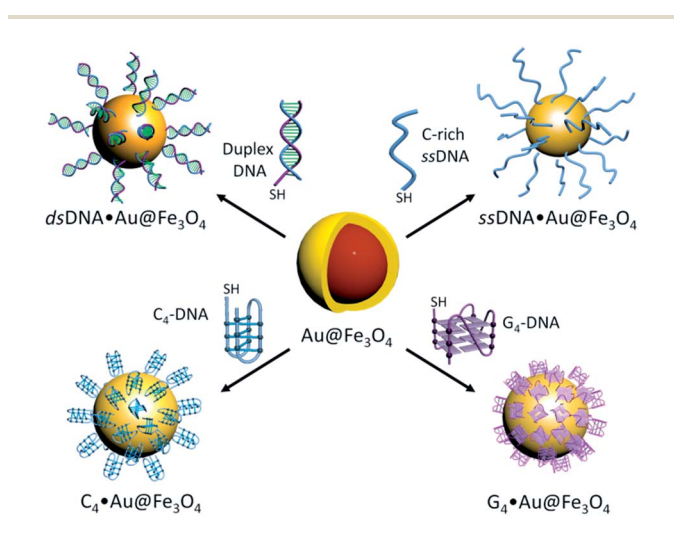


Fig. 1 DNA functionalized nanotemplates; i-motifs (c-MYC and BCL2), G-quadruplexes (c-MYC and BCL2), double and C-rich single stranded DNA (dsDNA and ssDNA) functionalized gold coated magnetic nanoparticles.

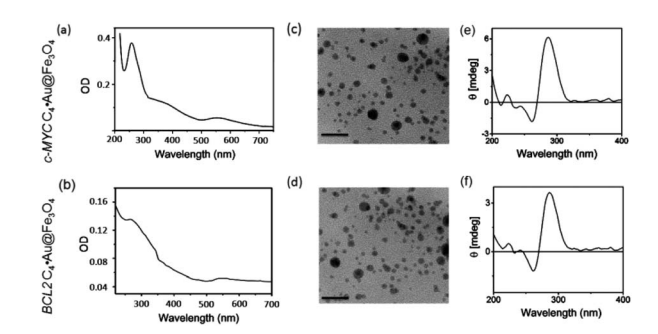


Fig. 2 Characterization of i-motif DNA linked magnetic nanoparticles (C₄·Au@Fe₃O₄ NPs). (a and b) UV-Vis absorption spectra of c-MYC $C_4 \cdot Au@Fe_3O_4$ and BCL2 $C_4 \cdot Au@Fe_3O_4$ NPs at 25 °C; (c and d) TEM images of c-MYC and BCL2 i-motif functionalized Au@Fe3O4 NPs (scale bar 50 nm); (e and f) CD spectra of c-MYC C_4 -Au@Fe $_3$ O $_4$ and BCL2 C₄·Au@Fe₃O₄ NPs; buffer: 10 mM sodium cacodylate, pH 5.5.

spherical in size and 13-15 nm in diameter (Fig. 2c and d). CD spectroscopy illustrated that DNA sequences grafted on nanoparticles retain i-motif conformation by displaying a positive peak at 285 nm and a negative peak at 260 nm (Fig. 2e and f). The complementary thiolated c-MYC and BCL2 G-rich sequences as well as a self-complementary dsDNA sequence were also immobilized on Au@Fe3O4 NPs to prepare G4 and dsDNA nanotemplates.

Design and synthesis of clickable building blocks

To perform metal free azide-alkyne cycloaddition using DNA nanotemplates, we developed a library of four water-soluble alkynes (1a-d) and seventeen azides (2a-q) containing different functional groups (Fig. 3). Two carbazole derived alkynes, containing an aryl carboxamide motif (1a)45 and a pyrrolidine motif (1b), an indole alkyne (1c) containing a pyrrolidine motif and a morpholino substituted benzamide alkyne derivative (1d) were prepared. The heteroaromatic ring system of alkynes could interact with DNA through π -stacking and their protonable amine side chains could participate in electrostatic interactions with the DNA sugar-phosphate backbone. The azide library consists of aliphatic and aromatic azides that include a range of functional groups such as amines (2a, 2b, 2e, 2h, and 2n), alcohols (2c and 2g), carboxylic acids (2d and 2j), an aldehyde (2i), an ester (2k), a nitro (2l), a simple phenyl azide (2f), meta- and para-substituted carboxamides (2o and 2p), an amino acid (2m) and a nucleoside (2q). These functional groups could promote hydrogen bonding, electrostatic or base stacking interactions with DNA targets. As shown in Fig. 3, the combinations of these azide and alkyne building blocks could provide 136 possible regioisomers that include both anti(1,4)- and syn(1,5)-triazoles. In the presence of a target, the in situ cycloaddition generally provides triazole products that effectively bind to the target via non-covalent interactions.

Lead discovery by DNA nanotemplated reactions

Each alkyne fragment (1 µM) was separately mixed with the azide library (4 µM of each azide fragment) in the presence of

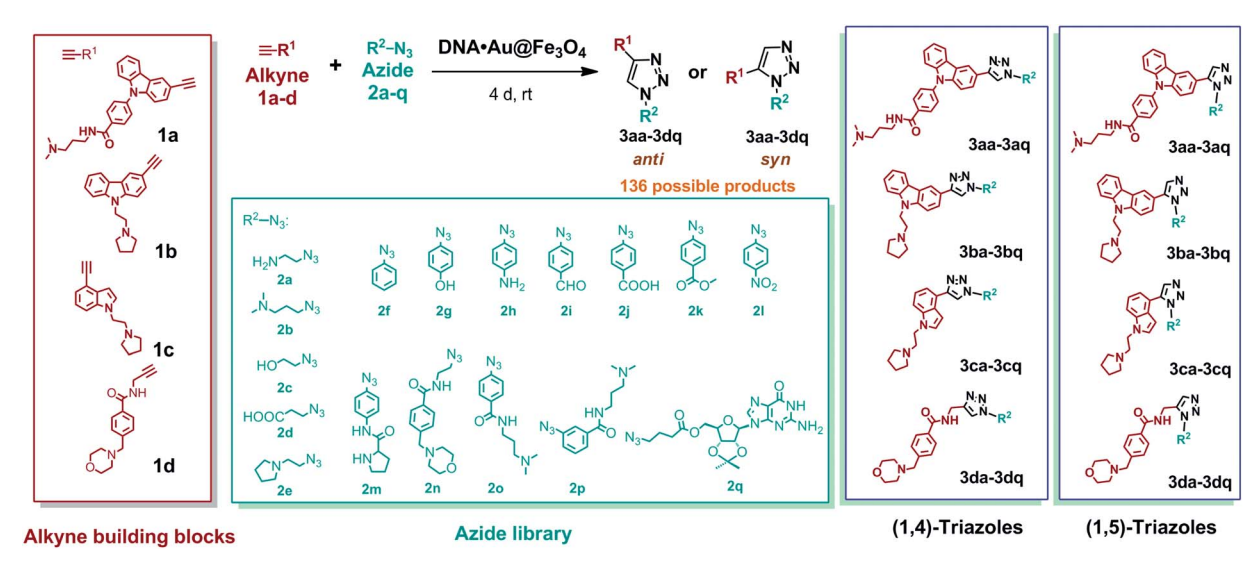


Fig. 3 Alkyne (1a-d) and azide (2a-q) fragments and regioisomeric 1,4-anti (3aa-3dq) and 1,5-syn (3aa-3dq) triazoles derived from combinations of alkyne and azide building blocks.

 $C_4\cdot Au@Fe_3O_4$ DNA nanotemplates (10 μL) in 10 mM sodium cacodylate buffer, pH 5.5 at rt (Fig. 4). The reaction vials were continuously mixed for 4 days and the newly ligated triazole products along with i-motif nanotemplates were separated from the unreacted fragments by washing with buffer followed by magnetic decantation. The triazole products were then separated from the nanotemplates by adding 1 M LiCl and heating the mixture at 65 °C in sodium cacodylate buffer (pH 5.5), followed by instant magnetic separation of the DNA nanotemplates. The combination of LiCl and heat destabilizes i-

motifs⁴⁷ and releases the bound triazole products from the DNA. The collected supernatants containing the products were characterized by HPLC-MS analysis. Control experiments were carried out using the same chemical library in the presence of c-MYC and BCL2 G₄ and dsDNA nanotemplates in 100 mM Tris-KCl buffer (pH 7.4).

The HPLC and MS analysis revealed that in the presence of c-MYC C_4 ·Au@Fe₃O₄, alkyne **1a** afforded three triazole hits, **3ab** (cycloadduct of **1a** and **2b**), **3ae** (cycloadduct of **1a** and **2e**), and **3an** (cycloadduct of **1a** and **2n**) in a ratio of 49 : 20 : 31 (Fig. 5a, c

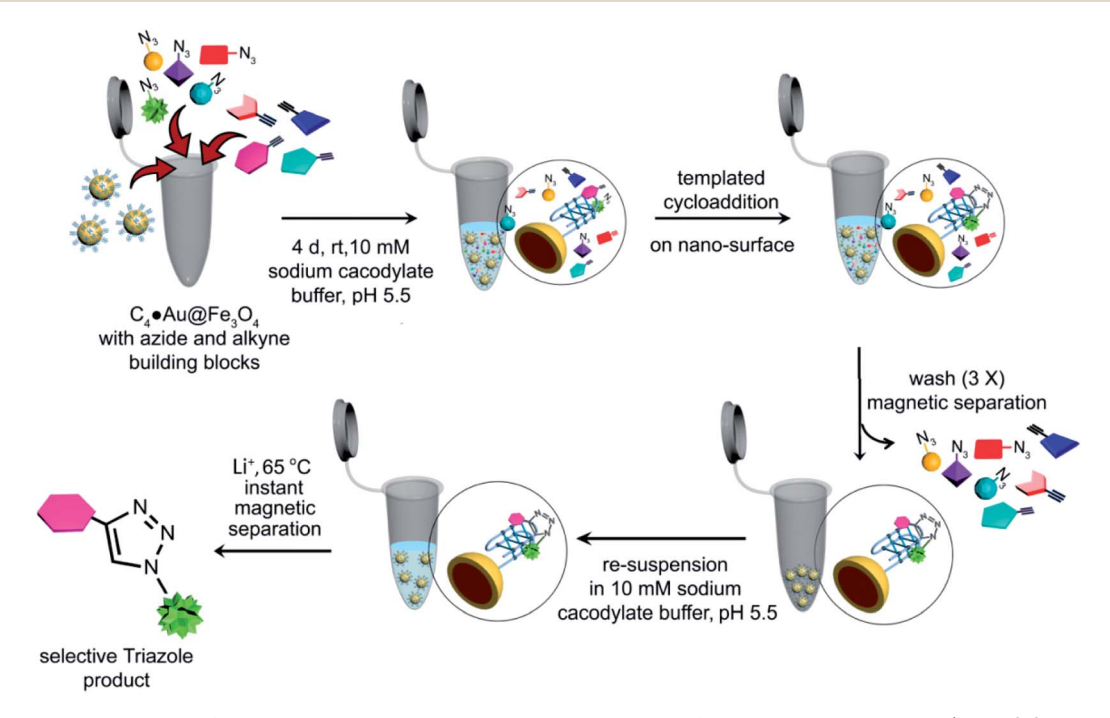


Fig. 4 Schematic representation of the target guided synthetic approach using i-motif magnetic nanotemplates (c-MYC C₄·Au@Fe₃O₄ & BCL2 C₄·Au@Fe₃O₄) for *in situ* formation of potent binders.

Edge Article

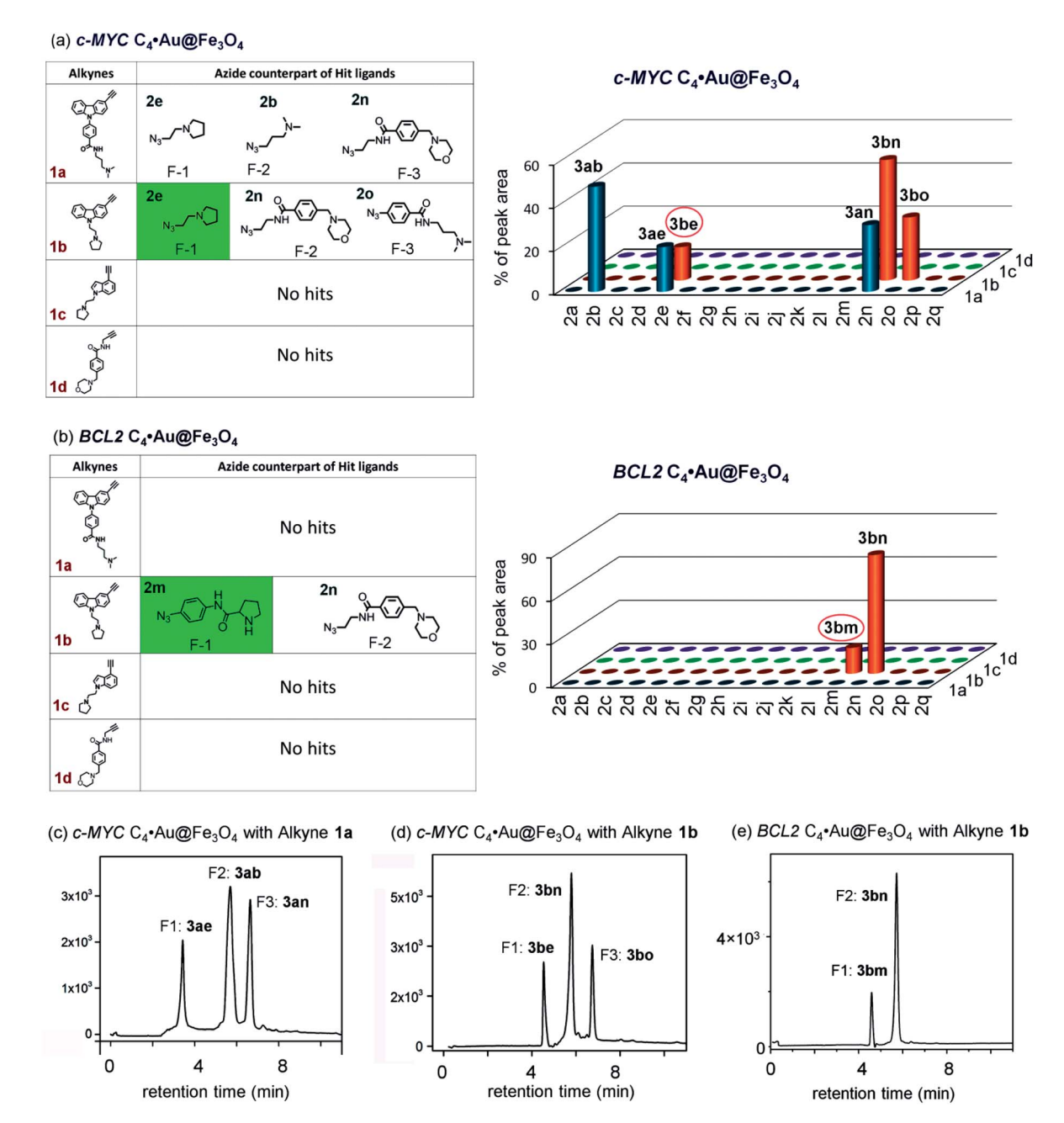


Fig. 5 The hit compounds formed using (a) c-MYC and (b) BCL2 $C_4 \cdot Au@Fe_3O_4$ templates. The selective lead compounds are highlighted. HPLC chromatograms of the products obtained (c and d) with c-MYC $C_4 \cdot Au@Fe_3O_4$ and (e) with BCL2 $C_4 \cdot Au@Fe_3O_4$.

and S5a, ESI‡); alkyne **1b** provided **3be**, **3bn** and **3bo** (15:56:29) (Fig. 5a, d and S5b, ESI‡); no hit products were obtained from alkynes **1c** and **1d** (Fig. 5a). In the presence of *BCL2* C₄·Au@Fe₃O₄, only alkyne **1b** afforded triazole products **3bm** and **3bn** in a ratio of 18:82 whereas no hit compounds were detected from alkynes **1a**, **1c** and **1d** (Fig. 5b, e and S5c, ESI‡).

In the control experiment with c-MYC G_4 · $Au@Fe_3O_4$, three hits (3ab, 3ae, and 3ao in a 13 : 9 : 78 ratio) were obtained from alkyne 1a and no product was obtained from alkynes 1b-d (Fig. 6a and S5c, ESI‡). The cycloaddition of azide-alkyne fragments in the presence of BCL2 G_4 · $Au@Fe_3O_4$ produced a single hit 3ap, derived from 1a and 2p (Fig. 6b and S5d‡). The

dsDNA nanotemplate provided 3 hits (3ab, 3ae and 3an in a ratio of 13:29:58) from alkyne 1a and 2 hits (3bn and 3bo in a 45:55 ratio) from alkyne 1b (Fig. S5f, g and S6‡). In addition, control experiments carried out with single-stranded c-MYC and BCL2 C-rich DNA sequences (ssDNA·Au@Fe₃O₄) immobilized on the nanoparticle surface (pH 7.4) showed no peaks in the HPLC chromatogram, indicating that C-rich ssDNA could not select the azide–alkyne fragments and promote the cycloaddition to generate any triazole product.

As azide fragments **20** and **2p** are positional isomers having identical molecular mass, the formation of **3bo**, **3ao** and **3ap** was confirmed by performing separate templated cycloaddition

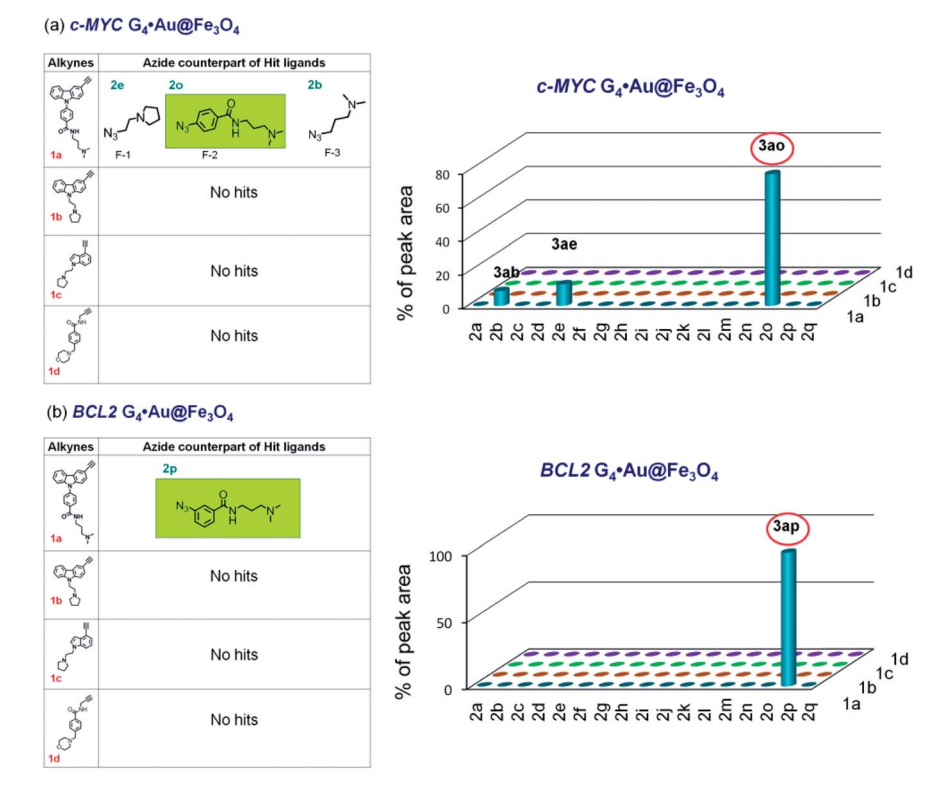


Fig. 6 The hit compounds formed using (a) c-MYC and (b) BCL2 G_4 ·Au@Fe $_3$ O $_4$ templates. The selective lead compounds are highlighted.

of the corresponding alkynes with the azides **20** or **2p** in the presence of the respective DNA nanotemplates. The c-MYC C₄- $Au@Fe_3O_4$ and dsDNA- $Au@Fe_3O_4$ produced **3bo** derived from **1b** and **2o** but no product was formed from **1b** and **2p**. By performing a similar set of cycloadditions, we observed that the c-MYC and BCL2 G₄- $Au@Fe_3O_4$ promoted the formation of **3ao** and **3ap** from azides **2o** and **2p**, respectively.

The comparison of hit products generated by using different DNA nanotemplates reveals that ligands **3be** and **3bm**, obtained using *c-MYC* and *BCL2* i-motifs, respectively, are selective leads for i-motifs, and ligands **3ao** and **3ap** are selective for *c-MYC* and *BCL2* G₄s, respectively. The other hit compounds are considered nonspecific as they were obtained using more than one DNA template.

Determination of the syn/anti selectivity of triazole leads

In order to determine the regiochemistry of selective triazole leads **3be**, **3bm**, **3ao** and **3ap**, the cycloaddition of their corresponding azide and alkyne fragments was carried out under thermal and Cu(ı)-catalyzed conditions (Fig. S2–S4⁺₇). A mixture of both *anti* (1,4)- and *syn* (1,5)-triazole regioisomers was obtained by thermal cycloaddition, and regioisomerically pure 1,4-disubstituted triazole products were formed by the Cu(ı)-assisted reaction. The comparison of the HPLC retention times of the DNA-templated reaction mixture with those of the triazole products obtained *via* thermal and Cu(ı)-catalyzed cycloaddition (Fig. S7–S10⁺₇) revealed that the DNA nanotemplates promote the cycloaddition of proximally oriented azide and alkyne fragments in a regioselective manner by preferentially generating *anti* (1,4)-triazole regioisomers for the DNA targets (Fig. 7).

The yields of lead *anti*-triazoles were determined by performing time dependent cycloaddition of corresponding alkyne (1a and 1b) and azide (2e, 2m, 2o and 2p) fragments in the presence of DNA nanotemplates. Alkyne 1b reacted with azide 2e in the presence of the *c-MYC* i-motif nanotemplate to form *anti-*3be in 48% yield. Similarly, leads *anti-*3bm (from 1b and 2m by using the *BCL2* i-motif), *anti-*3ao (from 1a and 2o using the *c-MYC* G-quadruplex) and *anti-*3ap (from 1a and 2p by using the *BCL2* quadruplex) were obtained in 60%, 44% and 56% relative yields, respectively (Fig. S11–S14, ESI‡).

Binding affinity and specificity of triazole leads for DNA targets

FRET-based DNA melting studies 48,49 using dual labelled *c-MYC* and *BCL2* i-motifs and G₄ DNA and dsDNA sequences revealed

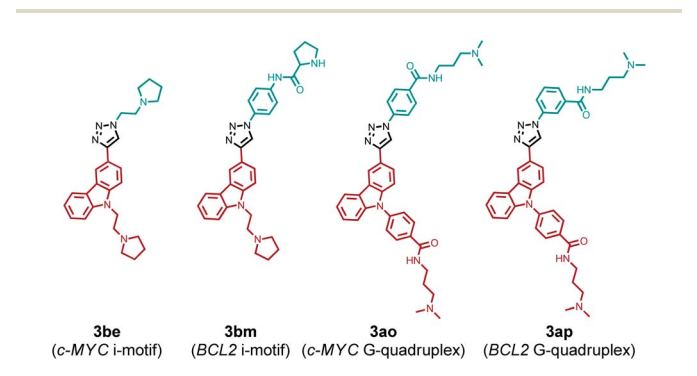


Fig. 7 Triazole leads formed *via in situ* cycloaddition promoted by DNA nanotemplates.

Edge Article Chemical Science

that ligand 3be, formed by using c-MYC C₄·Au@Fe₃O₄, showed a comparatively high preference for c-MYC i-motifs, exhibiting a $\Delta T_{\rm m}$ value of 29.7 °C at 1 μM concentration (Table 1, Fig. S15‡). The BCL2 i-motif lead 3bm shows a comparatively high $\Delta T_{\rm m}$ value (18.6 °C at 1 μ M) for the *BCL2* i-motif over other DNA structures. Ligand 3ao, generated using the c-MYC G₄-·Au@Fe₃O₄ nanotemplate, is found to exhibit high stabilization towards c-MYC G_4 ($\Delta T_m = 19.3$ °C at 1 μM) and 3ap exhibits a relatively high $\Delta T_{\rm m}$ value (11.8 °C at 1 μM) for BCL2 G₄ over other investigated DNAs. In addition, these triazole leads exhibit a weak stabilization potential for dsDNA illustrating their selectivity for four stranded structures over duplex DNA.

The binding selectivity of lead ligands was further validated by fluorescence spectroscopic titrations (Fig. 8 and S16,‡ Table

Table 1 Stabilization potentials ($\Delta T_{\rm m}$) and apparent dissociation constants $[K_{d(app)}]$ of lead triazole ligands for i-motif (C_4) , G-quadruplexe (G₄) and dsDNA as determined by the FRET based DNA melting assay and fluorescence spectroscopic titrations^f

	$\Delta T_{ m m}$ (°C) at 1 μ M ligand concentration				$K_{ m d(app)} \left(\mu { m M} ight)$			
	3be	3bm	Зао	Зар	3be	3bm	Зао	Зар
^a c-MYC C₄	29.7	2.9	6.4	2.1	0.25	ns	1.61	1.83
bBCL2 C_4	12.7	18.6	3.5	0.4	1.18	0.66	1.63	2.01
^c c-MYC G ₄	3.7	1.6	19.3	5.7	1.59	ns	0.17	1.62
d BCL2 G_4	1.8	1	7.7	11.8	2.21	ns	0.91	0.68
^e dsDNA	0.2	0.6	0.9	0.5	ns	ns	ns	ns

 a $T_{\rm m}$ for c-MYC C₄, 47.2 °C. b $T_{\rm m}$ for BCL2 C₄, 44.0 °C. c $T_{\rm m}$ for c-MYC G₄, 68.3 °C. d $T_{\rm m}$ for BCL2 G₄, 72.1 °C. e $T_{\rm m}$ for dsDNA, 63.4 °C. Buffer used for FRET melting studies; i-motif (C_4) DNA: 10 mM sodium cacodylate buffer (pH 5.5), G-quadruplex (G₄) and dsDNA: 60 mM potassium cacodylate buffer (pH 7.4). f ns: $K_{d(app)}$ could not be determined due to non-significant changes in fluorescence intensity upon addition of DNA. Experiments were performed in triplicate and the average values are provided.

1).50-54 As shown in Fig. 8, ligand 3be exhibited a binding preference for the *c-MYC* i-motif showing \sim 5-fold fluorescence quenching^{50,51} upon titration with *c-MYC* i-motif DNA. The fluorescence intensity of **3be** was quenched by only \sim 2-fold by the BCL2 i-motif and quadruplexes (c-MYC and BCL2). Moreover, this ligand showed negligible changes in the fluorescence intensity upon addition of dsDNA (Fig. S16‡).

Ligand 3bm, generated solely by using $BCL2 C_4 \cdot Au@Fe_3O_4$, showed \sim 2.0 fold fluorescence quenching along with a 20 nm blue shift in the presence of the BCL2 i-motif, while it showed negligible fluorescence changes with other DNA targets (Fig. S16‡). The observed quenching phenomenon for 3be and 3bm with i-motifs may be attributed to the possibility of resonance energy transfer between the DNA-bases and ligand which needs strong interactions between the molecules.⁵² The fluorescence intensity of ligand 3ao was enhanced 4-fold with a blue shift of 33 nm in the presence of c-MYC quadruplex DNA (Fig. S16[‡]) whereas a 2–2.5 fold enhancement was observed with other quadruplexes and i-motifs. A 5-fold fluorescence enhancement for 3ap was observed with a 15 nm red shift in the presence of BCL2 quadruplex DNA, whereas relatively lower fluorescence enhancement (3-3.5 fold) was obtained with other DNAs (Fig. S16[‡]). The significant fluorescence enhancement observed for compounds 3ao and 3ap indicated their binding with the hydrophobic sites of the G₄-DNA by stacking interactions.53,54

The apparent dissociation constants $[K_{d(app)}]$ determined from fluorimetric titrations revealed that ligand 3be binds the c-MYC i-motif with an apparent K_d value of 0.25 µm, which is 5-9 fold higher than the K_d values determined for other investigated i-motif and G₄-DNA targets. Triazole 3bm binds the BCL2 imotif with a dissociation constant (K_d) of 0.66 μM while showing no significant fluorescence response with other DNAs. The affinity of **3ao** for *c-MYC* G_4 ($K_d = 0.17 \mu M$) is about 5–10 fold higher than that for i-motifs and BCL2 G₄-DNA. Ligand 3ap

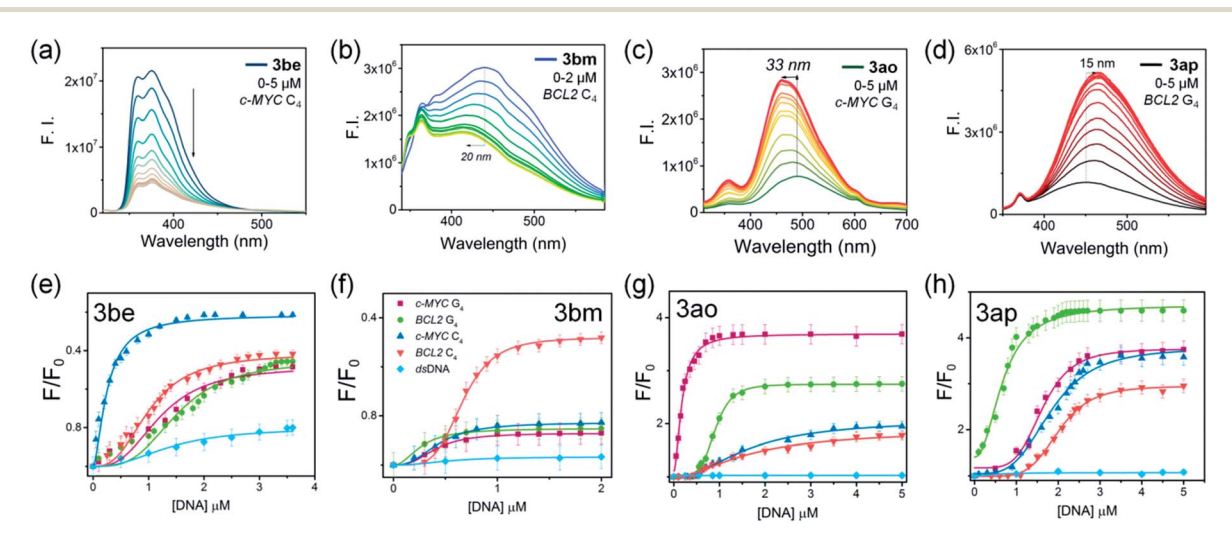


Fig. 8 (a-d) Fluorescence spectroscopic titrations of lead ligands (1 μ M) with c-MYC C₄, BCL2 C₄, c-MYC G₄ and BCL2 G₄ DNA. (e-h) Fluorescence spectroscopic titrations of lead ligands (1 μ M) with c-MYC C₄, BCL2 C₄, c-MYC G₄ and BCL2 G₄ DNA. (e-h) Fluorescence spectroscopic titrations of lead ligands (1 μ M) with c-MYC C₄, BCL2 C₄, c-MYC G₄ and BCL2 G₄ DNA. (e-h) Fluorescence spectroscopic titrations of lead ligands (1 μ M) with c-MYC C₄, BCL2 C₄, c-MYC G₄ and BCL2 G₄ DNA. rescence response curves of 3be, 3bm, 3ao and 3ap with incremental addition of c-MYC C4 (blue), BCL2 C4 (orange), c-MYC G4 (purple), BCL2 G₄ (green) and dsDNA (light blue).

also showed higher binding affinity for *BCL2* G_4 –DNA (K_d = 0.68 μ M) in comparison to other DNA targets (Table 1).

Chemical Science

Next, we performed a competitive binding assay55 using the DNA nanotemplates to further verify the selectivity of the lead compounds. The triazole leads (3be, 3bm, 3ao and 3ap) were mixed in an equimolar concentration (each ligand concentration is 5 µM) and incubated with each i-motif and G-quadruplex nanotemplate (C₄·Au@Fe₃O₄ and G₄·Au@Fe₃O₄) separately for 30 min at room temperature under continuous stirring. The underlying principle of the assay is to select the structureselective ligands using the DNA template from the mixture of lead triazole ligands and thus the captured ligand can be considered a specific and selective ligand for the respective DNA target. After incubation, the template-bound ligands were isolated from the template as per the protocol used in TGS and identified by HPLC and MS-analysis. The competitive binding experiments show that the c-MYC C₄·Au@Fe₃O₄ nanotemplate selected only **3be** from the mixture of four triazoles (Fig. S17a‡). Interestingly, as expected, the experiments carried out with the other three DNA nanotemplates showed a single peak in the HPLC chromatogram that corresponds to ligands 3bm, 3ao and 3ap for BCL2 C₄·Au@Fe₃O₄, c-MYC G₄·Au@Fe₃O₄ and BCL2 G₄·Au@Fe₃O₄, respectively (Fig. S17b-d‡). These results further confirm that the triazole leads obtained by TGS are specific to their respective DNA that drives their formation from their corresponding azide and alkyne fragments.

1D ¹H NMR titration further revealed that incremental addition of ligand 3be to the c-MYC i-motif results in general line broadening of the characteristic imino signals (15–16 ppm) for C-C⁺ base pairs (Fig. S18a, ESI[‡]). Furthermore, it induces significant line broadening in the aromatic region of the *c-MYC* i-motif (Fig. S18b‡), indicating that **3be** interacts with the *c-MYC* i-motif. In the absence of the ligand, NMR signals of the BCL2 imotif are broadened due to intermediate chemical exchange showing conformational dynamics of the DNA alone. Thus, no observable changes are found with addition of 3bm. 1D NMR titrations further revealed that ligand 3ao strongly interacts with c-MYC G₄ (Fig. S18g-i[‡]) showing significant line broadening suggesting binding in intermediate exchange on NMR time scale. In the case of 3ap, general line broadening of the imino and aromatic signals of BCL2 G4 in a 3:1 ligand/DNA molar ratio was observed indicating binding with a K_d in the high micro molar regime (Fig. S18j-l[‡]). CD spectroscopic titrations confirmed that these ligands retain the topology of these four stranded DNA targets (Fig. S19, ESI‡).

The results reveal that the $\Delta T_{\rm m}$ values and $K_{\rm d}$ values of triazole leads for DNA targets obtained from FRET melting and fluorescence spectroscopic titrations are in good agreement with each other. These results are consistent with the results obtained by TGS, indicating that a triazole lead shows selectivity for the DNA target that promotes its formation. For instance, ${\bf 3be}$ obtained using the c-MYC i-motif shows a high stabilization potential and high binding affinity for the c-MYC i-motif compared to other DNA targets. In summary, ligands ${\bf 3be}$ and ${\bf 3ao}$ displayed high affinity and specificity for the c-MYC i-motif and G-quadruplex DNA, respectively. In contrast, ligand ${\bf 3bm}$ and ${\bf 3ap}$ exhibited modest binding affinity for the BCL2 i-motif

and *BCL2* G-quadruplex DNA, respectively, but maintained considerable specificity for their respective DNA targets in comparison to other investigated DNA targets.

In vitro biological activity of triazole leads

The cytotoxicity of lead compounds was next evaluated in a human cervical cancer cell line (HeLa), a small lung adenocarcinoma cell line (A549), the BCL2 overexpressing EBV infected marmoset cell line B95.8 and the human normal kidney epithelial cell line NKE. It was observed that 3be, 3ao and 3ap inhibit cell proliferation in all the tested cancer cells (HeLa, A549 and B95.8) while they show minimal cytotoxicity towards the NKE cell line. The BCL2 i-motif lead 3bm is nontoxic to both normal and cancer cell lines (Table 2 and Fig. S20‡). The cellular localization of these triazole leads was then monitored in HeLa cells by confocal microscopy. It was observed that ligand 3ao (c-MYC G-quadruplex lead) exclusively localizes in the cell nucleus, and ligands 3be, 3bm and 3ap penetrate into the cell cytoplasm and the cell nucleus. This suggests that these triazole leads are able to translocate into the cell nucleus (Fig. S21, ESI‡). The ability of these ligands to induce apoptosis in cancer cells was further evaluated by annexin V/PI double staining FACS analysis. FACS analysis indicated that ligands 3be, 3ao and 3ap induced significant apoptotic cell death in HeLa cells in a dosedependent manner (Fig. S22‡). In comparison, the BCL2 imotif lead 3bm did not induce apoptosis in HeLa cells at 2 and 4 µM concentrations.

The qRT-PCR and western blotting results showed that the c-MYC i-motif and G_4 leads $3\mathbf{be}$ and $3\mathbf{ao}$ significantly reduce c-MYC expression at both the transcriptional and translational levels in HeLa and B95.8 cell lines (Fig. 9a, d and S23‡). However, these ligands ($3\mathbf{be}$ and $3\mathbf{ao}$) could not considerably suppress BCL2 gene expression in cancer cells. The BCL2 G-quadruplex ligand $3\mathbf{ap}$ inhibits the transcription and translation of the BCL2 gene while the BCL2 i-motif lead $3\mathbf{bm}$ upregulates BCL2 gene expression in both cancer cell lines (Fig. 9a, d and S23‡). In addition, it was observed that ligands $3\mathbf{bm}$ and $3\mathbf{ap}$ could not alter the c-MYC gene expression.

Dual luciferase promoter assays further illustrated that ligands **3be** and **3ao** selectively interact with the *c-MYC* G.C rich promoter region as the ligands could repress the firefly luciferase activity of the *c-MYC* promoter luciferase construct while

Table 2 IC_{50} values of lead compounds in human cancer cells and normal cells as measured using the XTT assay after 24 h of treatment^a

IC_{50} (μM)									
Ligands	HeLa	A549	B95.8	NKE					
3be	1.0	4.2	4.5	13.6					
3bm	>50.0	>20.0	>50.0	>25.0					
3ao	1.9	3.0	4.9	25.0					
Зар	7.9	14.9	8.9	>25.0					

^a Three individual experiments were performed and the average values are presented.

Edge Article Chemical Science

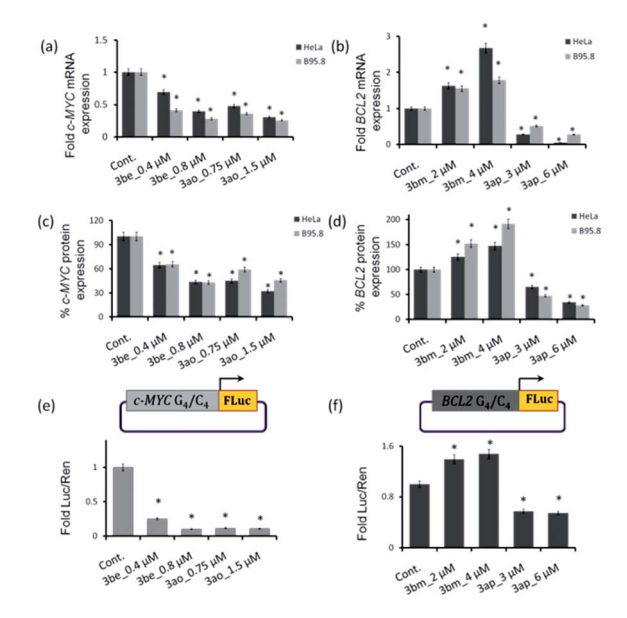


Fig. 9 (a-d) qRT-PCR and western blotting analysis results of c-MYC and BCL2 gene expression in HeLa and B95.8 cells after 24 h of treatment with 3be, 3bm, 3ao and 3ap. The in vitro dual luciferase promoter assay for evaluating the effect of the lead ligands on the promoter activity of (e) the c-MYC-FLuc promoter and (f) BCL2-FLuc promoter [*p value is < 0.05].

having a negligible effect on the transcriptional activity of the BCL2 promoter construct and normal B-DNA-containing luciferase construct (Fig. 9e, f and S24‡). The BCL2 i-motif binding ligand 3bm upregulates the transcriptional activity of the BCL2 promoter construct and has negligible effects on the expression levels of two other plasmid constructs. The BCL2 G-quadruplex lead 3ap could specifically inhibit the transcriptional activity of the BCL2 luciferase construct. These results establish that leads obtained by in situ cycloaddition can modulate c-MYC and BCL2 gene expression by interacting with G.C-rich promoter regions (Fig. 10).

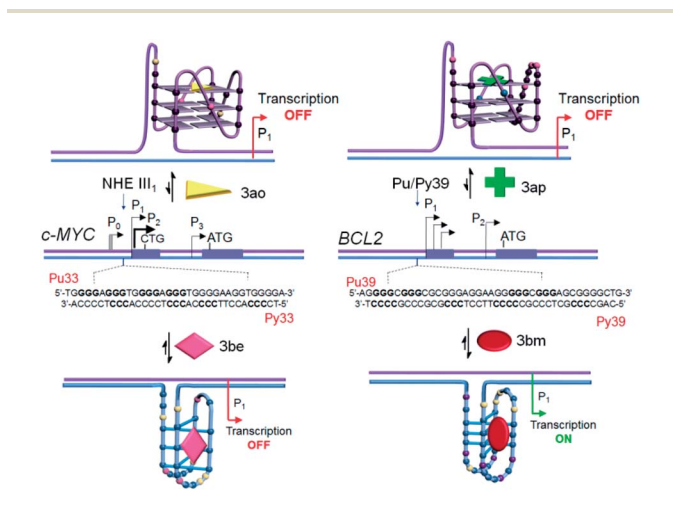


Fig. 10 Proposed model for targeting four-stranded DNA secondary structures within the c-MYC and BCL2 gene promoter regions

Conclusions

This study illustrates that i-motif DNA nanotemplates, i.e., gold coated magnetic nanoparticles functionalized with c-MYC and BCL2 i-motifs, promote the metal-free synthesis of imotif specific ligands. In order to generate selective ligands for i-motifs over G-quadruplex and duplex DNAs, complementary c-MYC and BCL2 G-quadruplex DNA functionalized nanotemplates and a self-complementary duplex DNA functionalized nanotemplate are used as control templates. These nanotemplates generated multiple triazole hits, but triazoles selectively formed by using a particular i-motif DNA nanotemplate are considered i-motif leads. The anti-triazole "lead" compounds 3be and 3bm generated using c-MYC and BCL2 imotifs, respectively, show high specificity for their targets as evidenced by FRET-melting, fluorescence titrations and competitive binding experiments. The control G-quadruplex nanotemplates also generated 3ao and 3ap as the lead compounds for c-MYC and BCL2 DNA quadruplexes, respectively. The lead compounds 3bm and 3ap obtained using the BCL2 i-motif and G-quadruplex, though they show moderate affinity, exhibit high specificity for their respective DNA targets. Furthermore, cell-based biological assays reveal that these leads can modulate the transcription of c-MYC and BCL2 genes. The c-MYC i-motif and G-quadruplex leads 3be and **3ao** significantly reduce the *c-MYC* expression without affecting the BCL2 expression. The BCL2 G-quadruplex lead 3ap downregulates BCL2 gene expression while the BCL2 imotif lead 3bm upregulates the expression of the BCL2 gene by directly stabilizing the G-C rich non-canonical DNA structures. Thus, the TGS approach using DNA nanotemplates facilitates cost-effective and rapid synthesis of highly potent and selective drug candidates for biomolecular targets. Based on the binding characteristics of the lead compounds, we are currently diversifying our chemical library to expand this strategy for the development of more promising drug candidates that may display high binding affinity and specificity for the targets of interest. Furthermore, the underlying principles of the observed transcriptional alterations imposed by the lead compounds are currently under investigation.

Conflicts of interest

There are no conflicts to declare.

Acknowledgements

JD thanks Wellcome Trust-DBT India Alliance [Grant Number, IA/S/18/2/503986] for funding. The authors thank Professor Shankar Balasubramanian for useful suggestions. J. D. thanks DST for a SwarnaJayanti fellowship and A. M. thanks DST for INSPIRE fellowships. The work was supported by DFG: CRC902 and by iNEXT, project number 653706, funded by the Horizon 2020 program of the European Union. Work at BMRZ is supported by the state of Hesse.

References

Chemical Science

- 1 T. A. Brooks, S. Kendrick and L. Hurley, *FEBS J.*, 2010, 277, 3459–3469.
- 2 S. Kendrick and L. H. Hurley, Pure Appl. Chem., 2010, 82, 1609–1621.
- 3 E. P. Wright, J. L. Huppert and Z. A. E. Waller, *Nucleic Acids Res.*, 2017, 45, 2951–2959.
- 4 J. X. Dai, E. Hatzakis, L. H. Hurley and D. Z. Yang, *PLoS One*, 2010, 5, e11647.
- 5 C. Sutherland, Y. X. Cui, H. B. Mao and L. H. Hurley, J. Am. Chem. Soc., 2016, 138, 14138–14151.
- 6 S. Kendrick, Y. Akiyama, S. M. Hecht and L. H. Hurley, *J. Am. Chem. Soc.*, 2009, **131**, 17667–17676.
- 7 S. Kendrick, H. J. Kang, M. P. Alam, M. M. Madathil, P. Agrawal, V. Gokhale, D. Z. Yang, S. M. Hecht and L. H. Hurley, J. Am. Chem. Soc., 2014, 136, 4161–4171.
- 8 R. V. Brown, T. Wang, V. R. Chappeta, G. H. Wu, B. Onel, R. Chawla, H. Quijada, S. M. Camp, E. T. Chiang, Q. R. Lassiter, C. Lee, S. Phanse, M. A. Tumidge, P. Zhao, J. G. N. Garcia, V. Gokhale, D. Z. Yang and L. H. Hurley, *J. Am. Chem. Soc.*, 2017, 139, 7456–7475.
- 9 C. E. Kaiser, N. A. Van Ert, P. Agrawal, R. Chawla, D. Z. Yang and L. H. Hurley, J. Am. Chem. Soc., 2017, 139, 8522–8536.
- 10 G. Miglietta, S. Cogoi, E. B. Pedersen and L. E. Xodo, *Sci. Rep.*, 2015, 5, 18097.
- 11 K. Guo, V. Gokhale, L. H. Hurley and D. Sun, *Nucleic Acids Res.*, 2008, **36**, 4598–4608.
- 12 K. Guo, A. Pourpak, K. Beetz-Rogers, V. Gokhale, D. Sun and L. H. Hurley, J. Am. Chem. Soc., 2007, 129, 10220–10228.
- 13 Y. Xu and H. Sugiyama, Nucleic Acids Res., 2006, 34, 949-954.
- 14 K. Gehring, J. L. Leroy and M. Gueron, *Nature*, 1993, 363, 561–565.
- 15 J. L. Leroy, M. Gueron, J. L. Mergny and C. Helene, *Nucleic Acids Res.*, 1994, 22, 1600–1606.
- 16 J. Choi, S. Kim, T. Tachikawa, M. Fujitsuka and T. Majima, J. Am. Chem. Soc., 2011, 133, 16146–16153.
- 17 L. A. Yatsunyk, O. Mendoza and J. L. Mergny, Acc. Chem. Res., 2014, 47, 1836–1844.
- 18 Z. G. Wang, J. Elbaz and I. Willner, *Nano Lett.*, 2011, **11**, 304–309.
- 19 T. Li and M. Famulok, *J. Am. Chem. Soc.*, 2013, **135**, 1593–1599.
- 20 S. Modi, M. G. Swetha, D. Goswami, G. D. Gupta, S. Mayor and Y. Krishnan, *Nat. Nanotechnol.*, 2009, **4**, 325–330.
- 21 H. Abou Assi, M. Garavis, C. Gonzalez and M. J. Damha, *Nucleic Acids Res.*, 2018, **46**, 8038–8056.
- 22 H. A. Day, P. Pavlou and Z. A. E. Waller, *Bioorg. Med. Chem.*, 2014, 22, 4407–4418.
- 23 M. Debnath, K. Fatma and J. Dash, *Angew. Chem., Int. Ed.*, 2019, **58**, 2942–2957.
- 24 S. Neidle, J. Med. Chem., 2016, 59, 5987-6011.
- 25 R. Hansel-Hertsch, M. Di Antonio and S. Balasubramanian, *Nat. Rev. Mol. Cell Biol.*, 2017, **18**, 279–284.
- 26 S. Asamitsu, T. Bando and H. Sugiyama, *Chem.–Eur. J.*, 2019, **25**, 417–430.

- 27 O. Y. Fedoroff, A. Rangan, V. V. Chemeris and L. H. Hurley, *Biochemistry*, 2000, 39, 15083–15090.
- 28 L. H. Wang, Y. B. Wu, T. G. Chen and C. Y. Wei, *Int. J. Biol. Macromol.*, 2013, **52**, 1–8.
- 29 L. A. Xue, N. Ranjan and D. P. Arya, *Biochemistry*, 2011, 50, 2838–2849.
- 30 D. L. Ma, M. H. T. Kwan, D. S. H. Chan, P. Lee, H. Yang, V. P. Y. Ma, L. P. Bai, Z. H. Jiang and C. H. Leung, *Analyst*, 2011, 136, 2692–2696.
- 31 R. R. Gao, S. Shi, Y. Zhu, H. L. Huang and T. M. Yao, *Chem. Sci.*, 2016, 7, 1853–1861.
- 32 I. J. Lee, S. P. Patil, K. Fhayli, S. Alsaiari and N. M. Khashab, *Chem. Commun.*, 2015, **51**, 3747–3749.
- 33 L. J. Xu, S. N. Hong, N. Sun, K. W. Wang, L. Zhou, L. Y. Ji and R. J. Pei, *Chem. Commun.*, 2016, 52, 179–182.
- 34 E. P. Wright, H. A. Day, A. M. Ibrahim, J. Kumar, L. J. E. Boswell, C. Huguin, C. E. M. Stevenson, K. Pors and Z. A. E. Waller, *Sci. Rep.*, 2016, **6**, 39456.
- 35 M. Debnath, S. Ghosh, A. Chauhan, R. Paul, K. Bhattacharyya and J. Dash, *Chem. Sci.*, 2017, **8**, 7448–7456.
- 36 B. Shu, J. J. Cao, G. T. Kuang, J. Qiu, M. L. Zhang, Y. Zhang, M. X. Wang, X. Y. Li, S. S. Kang, T. M. Ou, J. H. Tan, Z. S. Huang and D. Li, *Chem. Commun.*, 2018, 54, 2036–2039.
- 37 S. Dzatko, M. Krafcikova, R. Hansel-Hertsch, T. Fessl, R. Fiala, T. Loja, D. Krafcik, J. L. Mergny, S. Foldynova-Trantirkova and L. Trantirek, *Angew. Chem., Int. Ed.*, 2018, 57, 2165–2169.
- 38 M. Zeraati, D. B. Langley, P. Schofield, A. L. Moye, R. Rouet, W. E. Hughes, T. M. Bryan, M. E. Dinger and D. Christ, *Nat. Chem.*, 2018, **10**, 631–637.
- 39 R. Manetsch, A. Krasinski, Z. Radic, J. Raushel, P. Taylor, K. B. Sharpless and H. C. Kolb, *J. Am. Chem. Soc.*, 2004, 126, 12809–12818.
- 40 B. Farrow, M. Wong, J. Malette, B. Lai, K. M. Deyle, S. Das, A. Nag, H. D. Agnew and J. R. Heath, *Angew. Chem., Int. Ed.*, 2015, 54, 7114–7119.
- 41 I. Glassford, C. N. Teijaro, S. S. Daher, A. Weil, M. C. Small,
 S. K. Redhu, D. J. Colussi, M. A. Jacobson, W. E. Childers,
 B. Buttaro, A. W. Nicholson, A. D. MacKerell,
 B. S. Cooperman and R. B. Andrade, J. Am. Chem. Soc.,
 2016, 138, 3136-3144.
- 42 H. D. Agnew, R. D. Rohde, S. W. Millward, A. Nag, W. S. Yeo, J. E. Hein, S. M. Pitram, A. A. Tariq, V. M. Burns, R. J. Krom, V. V. Fokin, K. B. Sharpless and J. R. Heath, *Angew. Chem.*, *Int. Ed.*, 2009, 48, 4944–4948.
- 43 A. T. Poulin-Kerstien and P. B. Dervan, *J. Am. Chem. Soc.*, 2003, **125**, 15811–15821.
- 44 M. Di Antonio, G. Biffi, A. Mariani, E. A. Raiber, R. Rodriguez and S. Balasubramanian, *Angew. Chem., Int. Ed.*, 2012, 51, 11073–11078.
- 45 D. Panda, P. Saha, T. Das and J. Dash, *Nat. Commun.*, 2017, 8, 16103.
- 46 S. G. Rzuczek, H. Park and M. D. Disney, *Angew. Chem., Int. Ed.*, 2014, **53**, 10956–10959.
- 47 S. E. Kim, I. B. Lee, C. Hyeon and S. C. Hong, *J. Phys. Chem. B*, 2014, **118**, 4753–4760.
- 48 J. L. Mergny, Biochemistry, 1999, 38, 1573-1581.

49 A. De Cian, L. Guittat, M. Kaiser, B. Sacca, S. Amrane, A. Bourdoncle, P. Alberti, M. P. Teulade-Fichou, L. Lacroix

Edge Article

- A. Bourdoncle, P. Alberti, M. P. Teulade-Fichou, L. Lacroix and J. L. Mergny, *Methods*, 2007, **42**, 183–195.
- 50 I. Bessi, C. Bazzicalupi, C. Richter, H. R. A. Jonker, K. Saxena, C. Sissi, M. Chioccioli, S. Bianco, A. R. Bilia, H. Schwalbe and P. Gratteri, ACS Chem. Biol., 2012, 7, 1109–1119.
- 51 M.-P. Teulade-Fichou, C. Carrasco, L. Guittat, C. Bailly, P. Alberti, J.-L. Mergny, A. David, J.-M. Lehn and W. D. Wilson, *J. Am. Chem. Soc.*, 2003, 125, 4732–4740.
- 52 V. Kumar, A. Sengupta, K. Gavvala, R. K. Koninti and P. Hazra, *J. Phys. Chem. B*, 2014, **118**, 11090–11099.
- 53 J. Alzeer and N. W. Luedtke, *Biochemistry*, 2010, 49, 4339–4348.
- 54 V. Dhamodharan and P. I. Pradeepkumar, *ACS Chem. Biol.*, 2019, **14**, 2102–2114.
- 55 D. Panda, P. Saha, R. Chaudhuri, T. Prasanth, V. Ravichandiran and J. Dash, *Anal. Chem.*, 2019, **91**, 7705–7711.